# Measurement of *J* and Dipolar Couplings from Simplified Two-Dimensional NMR Spectra

Marcel Ottiger, Frank Delaglio, and Ad Bax

*Laboratory of Chemical Physics, National Institute of Diabetes and Digestive and Kidney Diseases,
National Institutes of Health, Bethesda, Maryland 20892-0520*

Simple procedures are described for recording complementary in-phase and antiphase *J*-coupled NMR spectra. The sum and difference of these spectra contain only the upfield and the downfield components of a doublet, making it possible to measure the *J* splitting directly from these combinations without an increase in resonance overlap relative to the decoupled spectrum. The approach is demonstrated for measurement of $^1J_{NH}$ splittings and $^2J_{HNC'}$ splittings in oriented and isotropic ubiquitin. Dipolar couplings obtained from differences in the splittings measured in the oriented and isotropic phases are in excellent agreement with dipolar couplings obtained from direct measurement of the splitting or from a conventional E.COSY-type measurement.

In recent years, considerable attention has focused on the development of methods for accurate measurement of *J* couplings. These include the widely used E.COSY (*1–4*) and quantitative *J* correlation (*4–7*) methods. A recently introduced modification of the E.COSY concept, referred to as spin-state-selective excitation or S$^3$E (*8, 9*), provides an even simpler and more convenient presentation of E.COSY-type data by generating two spectra, containing only resonances coupled to a given spin in the $|\alpha\rangle$ or in the $|\beta\rangle$ spin state. Other elegant methods for separately recording spectra containing these multiplet components have also been proposed (*10, 11*). Clean separation of the $|\alpha\rangle$ and $|\beta\rangle$ spin state spectra with the S$^3$E method is, however, quite sensitive to the size of the (one-bond) coupling used in separating the two types of signals. Although in isotropic protein solutions $^1J_{NH}$ couplings have very uniform values and are therefore well suited for this purpose, the spread in $^1J_{CH}$ values is somewhat larger. Moreover, with the recent introduction of a method for obtaining a tunable degree of molecular alignment relative to the magnetic field (*12, 13*), substantial variations in the size of both $^1J_{NH}$ and $^1J_{CH}$ occur. Here we report a simple method which also yields spin-state separated spectra, but which is less sensitive to the size of the coupling used for separating the signals. The method is applied to measurement of $^1J_{NH}$ and $^2J_{HNC'}$ splittings both in weakly oriented and in isotropic ubiquitin, and data are shown to

be in excellent agreement with those of direct measurement of $^1J_{NH}$ splittings and E.COSY measurement of $^2J_{HNC'}$.

Conceptually the simplest possible way to generate a $^1$H-coupled [$^{15}$N, $^1$H] correlation spectrum containing only the upfield (or downfield) $^{15}$N doublet component is to add two spectra: one recorded with in-phase doublets and one with antiphase doublets. For short, we refer to this as the IPAP approach. The regular $^1$H-coupled [$^{15}$N, $^1$H] heteronuclear single quantum correlation (HSQC) (*14*) generates in-phase doublets in the $F_1$ dimension. For a $^{15}$N spin, *S*, at an angular offset frequency $\delta$, coupled to its amide proton, *I*, antiphase *S* spin magnetization, $2I_zS_y$, is generated at the end of the first INEPT transfer. This then evolves according to

$$2I_zS_y \xrightarrow{t_1} 2\cos(\delta t_1)\cos(\pi J_{NH}t_1)I_zS_y$$
$$- 2\sin(\delta t_1)\cos(\pi J_{NH}t_1)I_zS_x + (\cdot\cdot\cdot)$$

$$\xrightarrow{90^\circ_x(I, S)} - 2\cos(\delta t_1)\cos(\pi J_{NH}t_1)I_yS_z + (MQ)$$

$$\xrightarrow{(2J_{NH})^{-1}} \cos(\delta t_1)\cos(\pi J_{NH}t_1)I_x,$$

where ($\cdot\cdot\cdot$) refers to the in-phase term present at the end of the $t_1$ evolution period, which does not get converted into observable *I*-spin magnetization, and (MQ) is unobservable two-spin coherence. The quadrature component in the $t_1$ dimension, obtained by incrementing the phase of the 90° *S*-spin pulse at the end of the first INEPT (*15*), starts with $-2I_zS_x$ at the beginning of the $t_1$ period and yields an observable $I_x$ magnetization modulated by $-\sin(\delta t_1)\cos(\pi J_{NH}t_1)$. So, the complex signal in the $t_1$ dimension equals $\cos(\pi J_{NH}t_1)[\cos(\delta t_1) - i\sin(\delta t_1)]I_x = \cos(\pi J_{NH}t_1)\exp(-i\delta t_1)I_x$.

A second HSQC experiment is then carried out where a $^{15}$N refocusing period $\Delta \approx (2J_{NH})^{-1}$ is inserted at the beginning of the evolution period (Fig. 1), and the phase of the first 90° *S* pulse is decremented by 90° relative to the regular HSQC experiment. Evolution during this period, terminated by a $^1$H purge pulse, is described by
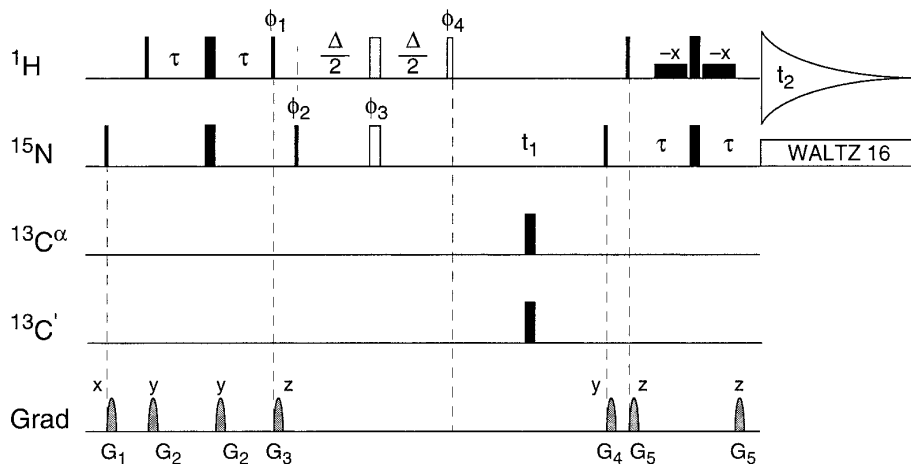
**FIG. 1.** Pulse scheme of the IPAP [$^{15}$N, $^{1}$H]-HSQC experiment. Narrow and wide pulses correspond to 90° and 180° flip angles, respectively, with phase $x$, unless indicated. The $\Delta/2-180°(^{1}\text{H}/^{15}\text{N})-\Delta/2-90°_{\phi4}$ sequence (open pulses) is only used in the experiment for generating the antiphase (AP) spectrum and is omitted for generating the in-phase (IP) spectrum. IP and AP spectra are recorded in an interleaved manner, and with the Bruker software version used (UXNMR 1.1), no gradients could be used around the $180°_{\phi3}$ $^{15}$N pulse. The low power $90°_{-x}$ pulses surrounding the final $^{1}$H 180° pulse are part of the WATERGATE solvent suppression scheme (*23*). $^{13}$C′ and $^{13}$C$^{\alpha}$ 180° pulses are applied to decouple $^{13}$C from $^{15}$N during $t_1$. These pulses are applied sequentially and have durations of $\sqrt{3}/(2\Delta\delta)$ (where $\Delta\delta$ is the frequency difference between the centers of the $^{13}$C$^{\alpha}$ and $^{13}$C′ regions). Delay durations: $\tau = 2.5$ ms; $\Delta = 5.3$ ms. All gradients are sine-bell shaped with 25 G/cm at their center. Gradient durations: $G_{1,2,3,4,5} = 2, 0.4, 2, 1, 0.4$ ms. Phase cycling: $\phi_1 = -y, y$; $\phi_2 = 2(x), 2(-x)$ for IP; $\phi_2 = 2(-y), 2(y)$ for AP; $\phi_3 = 4(x), 4(y), 4(-x), 4(-y)$; $\phi_4 = 8(x), 8(-x)$; Receiver $= x, 2(-x), x$ for IP; Receiver $= x, 2(-x), x, -x, 2(x), -x$ for AP. Quadrature detection in the $t_1$ dimension is obtained by altering $\phi_2$ (IP) or $\phi_2$ and $\phi_3$ simultaneously (AP) in the usual States–TPPI manner.

$$2I_zS_x \xrightarrow{\ \Delta/2-180°_x\,(I,S)-\Delta/2\ }$$

$$- 2R\cos(\pi J_{\text{NH}}\Delta)\,I_zS_x - R\sin(\pi J_{\text{NH}}\Delta)\,S_y$$

$$\xrightarrow{\ 90°_{,x}(I)\ } -R\sin(\pi J_{\text{NH}}\Delta)\,S_y,$$

where $R = \exp(-\Delta/T_2)$ denotes the decay as a result of $^{15}$N transverse relaxation. Note that interference between the $^{15}$N chemical shift anisotropy (CSA) and $^{15}$N–$^{1}$H dipolar coupling mechanisms (*16, 17*) has no net effect on the relative amplitude of the doublet components at the end of the $\Delta$ period because the amide proton spin state is inverted at the center of the $\Delta$ delay. Writing $Q = \sin(\pi J_{\text{NH}}\Delta)$, the in-phase $S$-spin subsequently evolves as

$$-RQS_y \xrightarrow{\ t_1\ } 2RQ\cos(\delta t_1)\sin(\pi J_{\text{NH}}t_1)\,I_zS_x$$

$$+ 2RQ\sin(\delta t_1)\sin(\pi J_{\text{NH}}t_1)I_zS_y + (\cdots)$$

$$\xrightarrow{\ 90°_x(I,S)\ } - 2RQ\sin(\delta t_1)\sin(\pi J_{\text{NH}}t_1)I_yS_z + (\text{MQ})$$

$$\xrightarrow{\ (2J_{\text{NH}})^{-1}\ } RQ\sin(\delta t_1)\sin(\pi J_{\text{NH}}t_1)I_x.$$

Similarly, a quadrature component in the $t_1$ dimension is obtained by incrementing the phase of the first $90°_{\phi2}$ $S$-spin

pulse and the following $180°_{\phi3}$ ($S$) pulse both by 90°, yielding a complex signal given by $RQ\,[\sin(\delta t_1) + i\,\cos(\delta t_1)]\sin(\pi J_{\text{NH}}t_1)\,I_x = i\,\sin(\pi J_{\text{NH}}t_1)\exp(-i\delta t_1)\,I_x$. Multiplying this signal by $(RQ)^{-1}$ and addition to the complex signal of the first experiment yields $\exp[-i(\delta - \pi J_{\text{NH}})t_1]\,I_x$. Similarly, subtraction of the two signals yields $\exp[-i(\delta + \pi J_{\text{NH}})t_1]$. Thus, Fourier transformation yields spectra with signals at either $\delta - \pi J_{\text{NH}}$ or $\delta + \pi J_{\text{NH}}$ in the $F_1$ dimension, i.e., separate spectra for the two doublet components. A simple pictorial way to visualize the separation of multiplet components is to add or subtract the signals of the two experiments at the beginning of the $t_1$ period (after multiplying the components in the second experiment by $1/RQ$), yielding $2I_zS_y \pm S_y$. These sum and difference terms are the product operator representations for the two $S$-spin doublet components.

The above combination of signals assumes $R$ and $Q$ are known. $R$ accounts for $^{15}$N spin relaxation during $\Delta$, and also includes a factor for signal loss resulting from imperfections of the two 180° pulses applied at the center of $\Delta$. As $\Delta$ is very short ($\sim$5.3 ms) relative to the $^{15}$N $T_2$, $R$ values typically fall in the range 0.95–0.85. The value for $Q = \sin(\pi J_{\text{NH}}\Delta)$ is rather insensitive to $J_{\text{NH}}$ and falls in the range 0.97–1 for $J_{\text{NH}}$ values that deviate by up to 16% from $1/2\Delta$. Therefore, the scaling factor $1/RQ$ is quite homogeneous for all residues and is easily optimized during data processing. To account for the difference in relaxation, one could insert
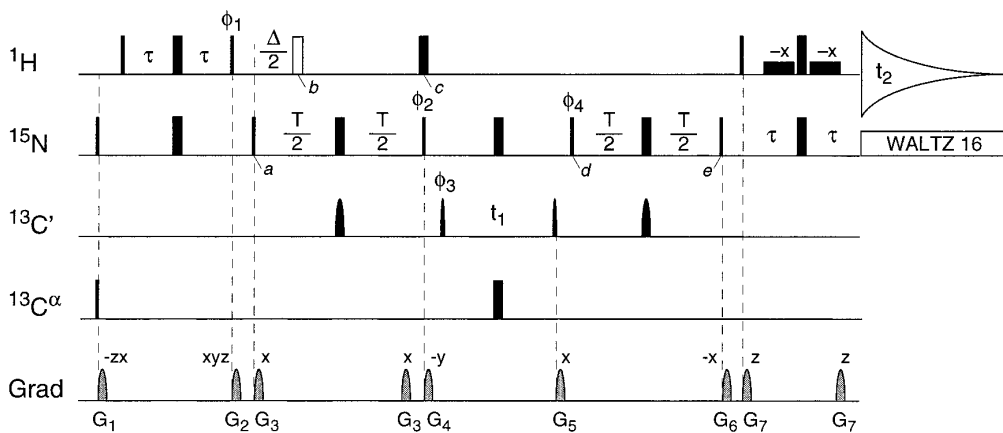
**FIG. 2.** Pulse scheme of the 2D IPAP-H(N)CO experiment. Narrow and wide pulses correspond to 90° and 180° flip angles, respectively, with phase $x$, unless indicated. The open 180°($^1$H) pulse at time point $b$ is only used in the experiment for generating the in-phase (IP) $^{13}$C′ spectrum and is omitted for generating the antiphase (AP) $^{13}$C′–{$^1$H$^N$} spectrum. The pulse width of the 180° $^{13}$C$^\alpha$ pulse is adjusted to $\sqrt{3}/(2\Delta\delta)$ (where $\Delta\delta$ is the frequency difference between the centers of the $^{13}$C$^\alpha$ and $^{13}$C′ regions), such that its excitation profile has a null at the $^{13}$C′ frequency. $^{13}$C′ pulses have the shape of the center lobe of a sin $x/x$ function, and have widths of 186 $\mu$s. Delay durations: $\tau = 2.5$ ms; $\Delta = 5.3$ ms; $T = 27$ ms. All gradients are sine-bell shaped with 25 G/cm at their center. Gradient durations: $G_{1,2,3,4,5,6,7} = 5, 1.1, 1, 0.5, 0.6, 0.7, 0.4$ ms. Phase cycling: $\phi_1 = -y, y$; $\phi_2 = 4(x), 4(-x)$ for IP, $\phi_2 = 4(y), 4(-y)$ for AP; $\phi_3 = 2(x), 2(-x)$; $\phi_4 = y$; Receiver = $x, 2(-x), x, -x, 2(x), -x$. Quadrature in the $t_1$ dimension is obtained by incrementing $\phi_3$ in the regular States–TPPI manner.

a $\Delta/2 - 180^\circ_y\,(^{15}\mathrm{N}) - \Delta/2$ period prior to $t_1$ evolution in the regular experiment. However, as the two $^{15}$N doublet components typically relax at different rates as a result of cross correlation between the dipolar and CSA relaxation mechanisms (*16, 17*), this would not completely eliminate the need to account for the effect of relaxation during this period.

Ignoring the effects of relaxation, for the IPAP method the intensity ratio of the suppressed over the selected doublet component is $[1 - \sin(\pi J\Delta)]/[1 + \sin(\pi J\Delta)]$. With $\Delta = (2J_{\text{target}})^{-1}$, $\phi = \pi(J - J_{\text{target}})\Delta$, and $|\phi| \ll \pi/2$, this ratio is approximately equal to $\phi^2/4$. For the S$^3$E method, the corresponding intensity ratio equals $\sin(\pi/4 - \pi J\tau/2)/\sin(\pi/4 + \pi J\tau/2)$. With $\tau = (2J_{\text{target}})^{-1}$, $\phi' = \pi(J - J_{\text{target}})\tau$, and $|\phi'| \ll 1$, this ratio is approximately equal to $-\phi'/2$. Thus, for $|(J - J_{\text{target}})/J_{\text{target}}| \ll 1$, the IPAP method is considerably less sensitive to small variations in $J$ than the S$^3$E method.

Analogous to the S$^3$E pulse sequence element, the IPAP method for separation of multiplet components is also easily implemented in many triple-resonance NMR experiments. One such implementation is shown in Fig. 2, which is a 2D version of the HNCO experiment (*18, 19*), correlating H$^N$ with the $^{13}$C′ of the preceding residue. In one experiment, **A**, the 180° pulse at time point $b$ is not applied, and the spin operator product term of interest at the start of the $^{13}$C′ $t_1$ evolution period is given by $4I_zS_zC_y$, where $I$, $S$, and $C$ are the spin operators for $^1$H$^N_i$, $^{15}$N$_i$, and $^{13}$C′$_{i-1}$, respectively. In the second experiment, **B**, with the 180° $^1$H pulse at time point $b$ included, the coherence of interest at the start of the $t_1$ evolution period equals $2QS_zC_y$, where $Q$ is again given by $Q = \sin(\pi J_{\text{NH}}\Delta)$. Adding (or subtracting) the two signals at

this point, after scaling the second one by $Q^{-1}$, yields the $^{13}$C′ multiplet component corresponding to H$^N$ in the $|\alpha\rangle$ (or $|\beta\rangle$) spin state. Thus, addition and subtraction of the signals obtained in the two experiments (after scaling by $Q^{-1}$) results in spectra in which only the $^{13}$C′–{$^1$H$^N = |\alpha\rangle$} or the $^{13}$C′–{$^1$H$^N = |\beta\rangle$} is present. These peak positions are separated by $^2J_{\text{HNC}'}$, which therefore is easily extracted from these two spectra, even in the case where $^2J_{\text{HNC}'}$ is much smaller than the $^{13}$C′ line width.

As mentioned above, as a result of interference between the dipolar and CSA relaxation mechanisms the $^{15}$N–{$^1$H$^N$} doublet components relax at different rates. Temporarily ignoring the fact that there is no net effect of relaxation interference during the $\Delta$ period in scheme **B**, the intensity of the added spectrum containing the $^{13}$C′–{$^1$H$^N = |\alpha\rangle$} signals would be weaker by a factor $\exp(-4T\eta)$ relative to the spectrum containing the $^{13}$C′–{$^1$H$^N = |\beta\rangle$} signals, where $\eta$ is the cross relaxation rate as defined by Goldman (*16*) and $T$ is the duration of the $^{15}$N–{$^{13}$C′} de- and rephasing intervals (Fig. 2). However, by inserting a 180° $^1$H pulse at time point $c$, a $^{15}$N-spin dephasing between time points $a$ and $c$ while attached to $^1$H$^N = |\alpha\rangle$ will rephase between time points $d$ and $e$ attached to a $^1$H$^N = |\beta\rangle$ spin and the **A** + **B** and **A** − **B** spectra will be of the same intensity. This argument ignores that in experiment **B**, with the 180° H$^N$ pulse at time $b$ included, the cross relaxation is effectively eliminated for the duration $\Delta$. Therefore, instead of equal intensity $^{13}$C′–{$^1$H$^N$} doublet components, the $^1$H$^N = |\alpha\rangle$ multiplet component will be more intense than the $^1$H$^N = |\beta\rangle$ component by a factor $\exp(2\eta\Delta)$. Thus, whereas in the first experiment (without the 180° $^1$H pulse at time point
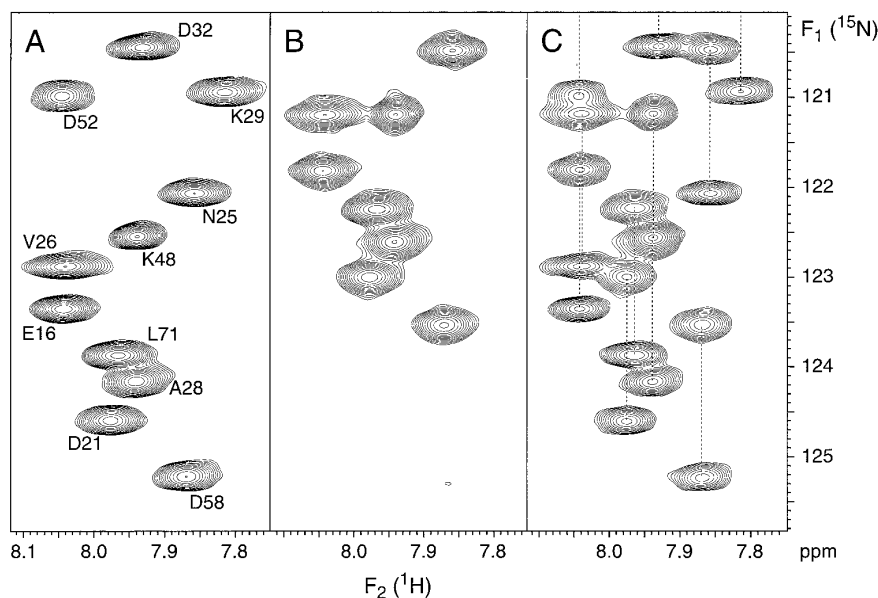
**FIG. 3.** Regions of the ubiquitin [$^{15}$N,$^1$H]-HSQC spectrum recorded in the liquid crystalline phase. (A) Downfield and (B) upfield doublet components of the IPAP-[$^{15}$N,$^1$H]-HSQC spectrum, obtained by (A) subtracting and (B) adding the in-phase and antiphase signals obtained with the pulse scheme of Fig. 1, using a scaling factor, $1/RQ = 1.11$ for the antiphase signals. For comparison, (C) shows the regular $^1$H-coupled [$^{15}$N, $^1$H]-HSQC spectrum. Note that the upfield doublet components are broader than the downfield components as a result of relaxation interference (*16, 17*).

*b*) the two doublet components have the same integrated intensity, in the second experiment their relative intensities are $\exp(\eta\Delta)$ and $\exp(-\eta\Delta)$, respectively. The value of $\eta$ scales linearly with the magnetic field strength, and at 600 MHz it is approximately 35% of the in-phase $^{15}$N transverse
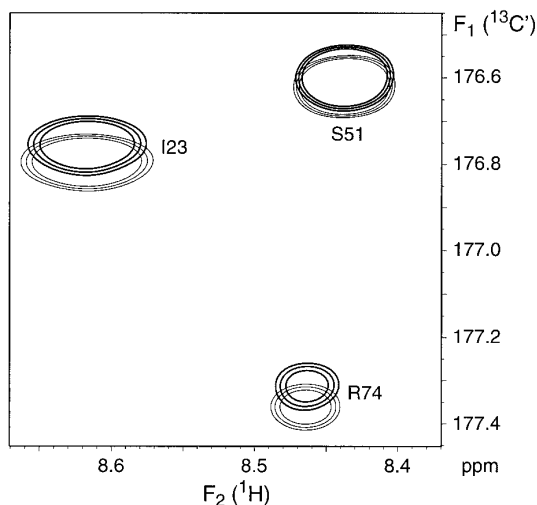


**FIG. 4.** Small region of superposition of the sum (thick contours) and the difference (thin contours) of the IP and AP spectra of the $^1$H$_i^N$-coupled $^{13}$C$_{i-1}$ − $^1$H$_i^N$ correlation spectrum of ubiquitin, recorded with the pulse scheme of Fig. 2 in the aligned state. The spectra result from two 300* × 1024* data matrices, recorded with 48 scans per complex $t_1$ increment (total measuring time 11 h).

relaxation rate. In practice, $\exp(\eta\Delta)$ is close to one, and it can be shown that omission of these $\exp(\eta\Delta)$ and $\exp(-\eta\Delta)$ correction factors shifts the $F_1$ frequency in spectra **A** + **B** and **A** − **B** in the same direction by approximately equal amounts. So, from a practical perspective, there is no need to correct for the effect of cross correlation during the $\Delta$ period.

Experiments were applied to measurement of $^1J_{\text{NH}}$ and $^2J_{\text{HNC}'}$ splittings in a 0.7 mM sample of U–$^{13}$C/$^{15}$N ubiquitin (VLI Research, Southeastern, PA), dissolved in 93% H$_2$O, 7% D$_2$O in a 250-$\mu$l Shigemi microcell, pH 6.6. The solution also contained 12.5 mg of dihexanoyl phosphatidylcholine (DHPC) and dimyristoyl phosphatidylcholine (DMPC) (Avanti Polar Lipids, Alabaster, AL) in a 1:3 molar ratio (*12, 13, 20*). All spectra were recorded on a Bruker DMX-600 spectrometer, both in the isotropic phase at 25°C, and in the liquid crystalline phase at 38°C.

Figure 3 shows small regions of the sum and difference [$^{15}$N,$^1$H]-HSQC spectra, recorded in the aligned state, using the pulse scheme of Fig. 1. The weighted sum and difference of the in-phase (IP) and antiphase (AP) HSQC yield spectra displaying the upfield and downfield $^{15}$N doublet components (Figs. 3A, 3B). For reference, Fig. 3C shows the corresponding region of the regular HSQC spectrum, coupled in the $F_1$ dimension. In Figs. 3A and 3B, suppression of the second doublet component is in all cases better than 96%. Thus, the effect of spectral overlap between the downfield component of one doublet with the upfield component of another one is minimized, and accurate values for the split-

tings can be obtained from the difference in $F_1$ frequencies for pairs of doublet components.

Figure 4 shows a small region of the 2D IPAP-H(N)CO spectrum, recorded with the scheme of Fig. 2. The resonances in the summed spectrum ($\mathbf{A} + \mathbf{B}$) are shown as thick contours, superimposed on the difference spectrum ($\mathbf{A} - \mathbf{B}$), shown as thin contours. The relative displacement of these peaks is again easily measured and corresponds to the sum of the two-bond $J_{HNC'}$ and $D_{HNC'}$ couplings. This splitting can also be measured in the $^1H$ dimension of a $^{13}C'$-coupled [$^{15}N$, $^1H$]-HSQC spectrum, when care is taken that the $^{13}C'$ is not perturbed during the experiment and an E.COSY-type correlation is obtained (21). Measurement of the splitting in the $^{13}C'$ dimension is considerably more accurate, however, because the $^{13}C'$ linewidth is more than threefold narrower than the $^1H^N$ linewidth. Note that in the aligned state, the $^1H^N$ resonance is broadened by incomplete averaging of homonuclear $^1H$–$^1H$ dipolar couplings (13), whereas the $^{13}C'$ resonance is much less affected by dipolar couplings to $^1H$.

Assuming that the $J$ contribution to the observed splittings does not change when shifting from the isotropic to the weakly aligned state, the dipolar contribution is readily obtained from the difference between the splittings in the aligned and isotropic states. Figure 5 demonstrates the excellent agreement obtained between dipolar $^1D_{NH}$ couplings (derived from the difference in splitting in the aligned and isotropic states) measured from the $F_1$ doublet splittings and with the IPAP method. As a result of the residual, very small second multiplet component, minute distortions in peak position of an overlapping selected multiplet component can occur. Therefore, the IPAP method does not offer as accurate a set of couplings as the $J$-modulated HSQC experiment (22), which yielded a precision of ±0.02 Hz. However, the dipolar splittings derived from the two separate measurements agree to within a pairwise root-mean-square difference of 0.16 Hz, indicating a precision of ~0.1 Hz for the individual measurements. Considering that in the liquid crystalline medium the dipolar couplings cover a range which is two orders of magnitude larger than in the magnetically aligned case, ultrahigh accuracy measurement of these dipolar couplings is no longer needed, and the convenience of the IPAP method makes it an attractive alternative to the intensity-modulated HSQC method (22).

Figure 5B compares the $^2D_{HNC'}$ splittings obtained with IPAP method with those of the $^{13}C'$-coupled [$^{15}N$, $^1H$]-HSQC spectrum. Clearly, even for the two-bond $^2D_{HNC'}$ interaction, the measurement uncertainty is considerably smaller than the range of values observed and yields a pairwise RMSD of only 0.38 Hz, and an error of less than 0.3 Hz in the individual measurements. This indicates that $^2D_{HNC'}$ can serve as a useful complement to the previously measured one-bond $D_{NH}$, $D_{CH}$, $D_{CC}$, and $D_{C'N}$ couplings in protein structure determination.
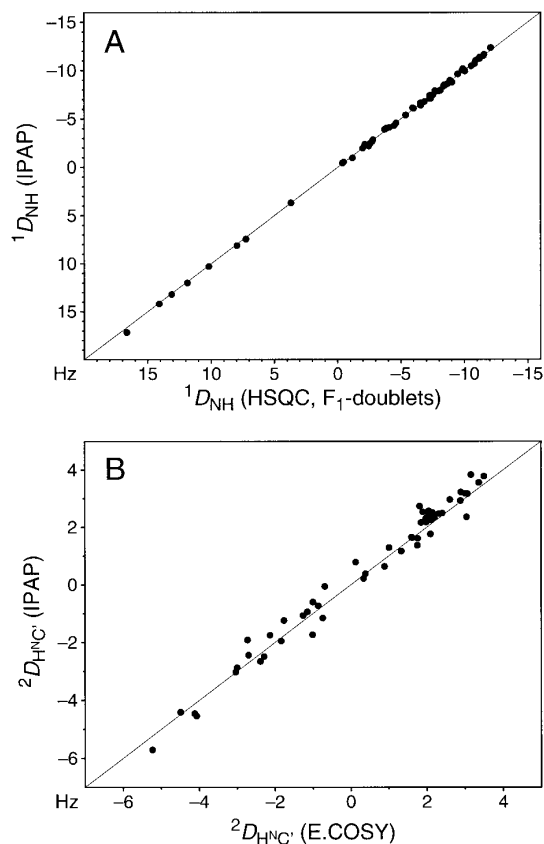


**FIG. 5.** Plots of dipolar couplings, $D$, measured with standard versus IPAP techniques. (A) $^1D_{NH}$ measured from $F_1$ doublets of a $^1H$-coupled [$^{15}N$, $^1H$]-HSQC spectrum (Fig. 3C) versus $^1D_{NH}$ from an IPAP-[$^{15}N$, $^1H$]-HSQC spectrum (Figs. 3A, 3B). (B) $^2D_{HNC'}$ measured from an E.COSY-type [$^{15}N$–{$^{13}C'$}, $^1H$]-HSQC spectrum versus $^2D_{HNC'}$ from an IPAP-H(N)CO spectrum (Fig. 4). The dipolar couplings are derived from the difference in splitting measured in the aligned state at 38°C and in the isotropic state at 25°C, assuming that the $J$ coupling contribution to the splitting is independent of temperature. The pairwise RMS deviations are 0.16 Hz for (A) and 0.38 Hz for (B). Due to the negative sign of the gyromagnetic ratio of $^{15}N$ the axis for $^1D_{NH}$ of (A) have been inverted.

The IPAP approach offers a convenient alternative to the widely used E.COSY technique and the more recent S$^3$E method, particularly when measuring couplings in isotopically enriched macromolecules where the large and relatively uniform one-bond $J$ couplings can be used to obtain clean separation of the in-phase and antiphase spectra. Our results indicate that heteronuclear dipolar couplings can also be measured conveniently with this approach, suggesting that such measurements will become increasingly important in molecular structure determination by NMR.

## ACKNOWLEDGMENTS

## REFERENCES

*1.* C. Griesinger, O. W. Sørensen, and R. R. Ernst, *J. Chem. Phys.* **85,** 6837 (1986).

*2.* G. T. Montelione and G. Wagner, *J. Am. Chem. Soc.* **111,** 5474 (1989).

*3.* C. Biamonti, C. B. Rios, B. A. Lyons, and G. T. Montelione, *Adv. Biophys. Chem.* **4,** 51 (1994).

*4.* A. C. Wang and A. Bax, *J. Am. Chem. Soc.* **118,** 2483 (1996).

*5.* A. Bax, D. Max, and D. Zax, *J. Am. Chem. Soc.* **114,** 6923 (1992).

*6.* J.-S. Hu and A. Bax, *J. Am. Chem. Soc.* **119,** 6360 (1997).

*7.* B. Reif, M. Köck, R. Kerssebaum, J. Schleucher, and C. Griesinger, *J. Magn. Reson. B* **112,** 295.

*8.* A. Meissner, J. Ø. Duus, and O. W. Sørensen, *J. Biomol. NMR* **10,** 89 (1997).

*9.* A. Meissner, J. Ø. Duus, and O. W. Sørensen, *J. Magn. Reson.* **128,** 92 (1997).

*10.* A. Ross, M. Czisch, and T. A. Holak, *J. Magn. Reson. A* **118,** 221 (1996).

*11.* T. Fäcke and S. Berger, *J. Magn. Reson. A* **119,** 260 (1996).

*12.* A. Bax and N. Tjandra, *J. Biomol. NMR* **10,** 289 (1997).

*13.* N. Tjandra and A. Bax, *Science* **278,** 1111 (1997).

*14.* G. Bodenhausen and D. J. Ruben, *Chem. Phys. Lett.* **69,** 185 (1980).

*15.* D. J. States, R. A. Haberkorn, and D. J. Ruben, *J. Magn. Reson.* **48,** 286 (1982).

*16.* M. Goldman, *J. Magn. Reson.* **60,** 437 (1984).

*17.* N. Tjandra, A. Szabo, and A. Bax, *J. Am. Chem. Soc.* **118,** 6986 (1996).

*18.* S. Grzesiek and A. Bax, *J. Magn. Reson.* **96,** 432 (1992).

*19.* J. Cavanagh, W. J. Fairbrother, A. G. Palmer III, and N. J. Skelton, ''Protein NMR Spectroscopy. Principles and Practice,'' p.499, Academic Press, San Diego (1995).

*20.* C. R. Sanders and J. P. Schwonek, *Biochemistry* **31,** 8898 (1992).

*21.* F. Delaglio, D.A. Torchia, and A. Bax, *J. Biomol. NMR* **1,** 439 (1991).

*22.* N. Tjandra, S. Grzesiek, and A. Bax, *J. Am. Chem. Soc.* **118,** 6264 (1996).

*23.* M. Piotto, V. Saudek, and V. Sklenar, *J. Biomol. NMR* **2,** 661 (1992).